JOURNAL OF MATERIALS SCIENCE **40** (2005) 2775–2782

A theoretical study of H absorption at a Fe(110)–Pd(100) interface and Fe–Pd alloys

P. V. JASEN, E. A. GONZALEZ, N. J. CASTELLANI, A. JUAN*
Departamento de Física, Universidad Nacional del Sur, Av. Alem 1253, Bahía Blanca (8000), Argentina
E-mail: cajuan@criba.edu.ar

The electronic structure and bonding at a Fe(110)–Pd(100) interface was theoretically analyzed in the framework of semi-empirical quantum chemical calculations. The Fe–Pd interface was modeled by a $Fe_{74}Pd_{74}$ cluster and a Fe–Pd six layer slab.

The extended Hückel tight binding (EHTB) method and its modifications, including repulsive interactions, were used to calculate the interfacial adhesion and the H-absorption energy.

The energetic minimum position for H is found at the Fe–Pd interface closer to the Pd layer.

The interfacial Fe–Pd distance result to be 1.73 Å where Fe–Pd develops a strong bonding interaction. An important metal–metal adhesion was also found.

The changes in the Density of States (DOS) and the Crystal Orbital Overlap Population (COOP) were compared in different structures: clusters, slab and two types of Fe–Pd alloys.

The H as an impurity is responsible for a Fe–Fe and Pd–Pd bond weakening. However, the H effect is much less detrimental for the Fe–Pd bonds at the interface.

When H is located at interstitial sites in bulk Fe–Pd alloys, the Pd–Pd overlap population shows a notorious decrease in the case of fcc structures while for fct structures the change is only 12%. The intermetallic bonding was also weakened as compared with the pure alloys. The objective of this work is to bring a plausible explanation to the null permeability to hydrogen in Pd-coated Fe films.

1. Introduction

The hydrogen-palladium alloy systems have been well studied due to their excellent interaction and properties. Nowadays, great attention has been paid to binary and ternary palladium alloys [1]. Pd-based alloys containing small amounts of oxidizable solute metals such as Al, Mg and Zn have been characterized using hydrogen as a probe [2]. Also there have been various studies of hydrogen absorbing properties in other metal–metal based alloy like $TiMn_2$ just to mention one [3].

The practical uses of metal–hydrogen systems include the ability of some metals and alloys to store hydrogen [4]. Hayashi *et al*. have reported experiments where palladium-coated Fe films have practically null permeability to hydrogen [5]. That is the reason why interfacial Fe–Pd studies have a critical technological importance. Furthermore, Fe/Pd multilayers are of particular interest because of an abnormally large Pauli susceptibility of the Pd atoms. Other wise, there is no visible interdiffusion of Fe into the Pd layer as well [6].

It is well known that the adsorption of atoms on transition metal (TM) surfaces can strongly influence their structural, electronic, catalytic and magnetic properties [7, 8]. Experiments on TM alloys and their compounds have shown unusual adsorption properties, different from those of the pure metal surface [10, 11]. A few theoretical investigations of gas adsorption onto intermetallic alloy surfaces have been carried out [9–13]. Hydrogen plays a crucial role in the properties of various materials and the modification of the surface electronic properties by hydrogen adsorption is still not completely understood. Despite intensive experimental investigations into the effect of hydrogenation on TM alloy surfaces, the interaction between adsorbed hydrogen and a TM is an open question [14].

While the technological importance of adhesion is well know, there have been a number of recent experimental reports that suggest that impurities can have a substantial effect on interfacial adhesion [15]. It has become increasingly important to gain a microscopic understanding of impurity effects in adhesion. First-principles studies of adhesion between different materials have focused on impurity-free interfacial contacts [16 and references there in].

A hydrogen atom implanted into the materials first diffuses from the implanted range to surface of both

*Author to whom all correspondence should be addressed.

the front and the backsides and then recombines with another atom to desorb as a H_2 molecule. The later process is often the rate-limiting process on both sides [17]. The coating effect on hydrogen permeation, therefore, has been studied by many authors [5, 18–20].

In the following sections, we will theoretically compare the Fe–Pd interface with Fe–Pd alloys. Then the changes in the electronic structures and bonding will be addressed. In this study we have modeled both a Fe–Pd cluster and a slab with the appropriate geometry to match both surfaces. The cluster approximation emphasizes local interactions while the slab calculations consider the extended nature of the interface. The comparison between these two configurations allows us to weight local vs. delocalized effects. The two types of FePd stable alloys structures are also analyzed and the H located at their interstitial sites of minimum energy. We have also used a model of cluster consisting in three Fe layers over a Pd substrate in agreement with Roos *et al*. in order to keep the crystalinity of the structure [6].

Extended Hückel (EH) like calculation method is particularly well suited to model the extended, two-dimensional nature of interface and to study the effect of variations in interface geometry on the overall energy of a structure. Specifically, this molecular orbital method includes calculation of the overlap population (an index of bond strength) for the interface. Calibration of such bond strength indexes is possible by comparison with similar calculations performed on bulk materials. To acquire more detailed information on the binding energies of this system with H an Atom Superposition and Electron Delocalization Molecular Orbital (ASED-MO) calculation has also been performed. This method provides a good first approximation to the relative stability of adsorption (or absorption) sites on TM and has been widely used as a *comparative* tool [21–23]. Computational details are given in the Appendix.

2. Models for the interface and structures

2.1. Fe_{74}–Pd_{74} cluster

Solid α-Fe has a bcc structure with a lattice parameter a, for the unit cell, of 2.861 Å while solid Pd has one of 3.89 Å in fcc structure. Looking for a geometrical match between low index planes, the (110) and (100) faces for Fe and Pd were chosen respectively. The Pd layers were rotated 45° respect to the Fe layers. Several other relative rotations between Fe and Pd layers were made and no significative changes for the total energy were found. We have simulated two Fe(110)–Pd(100) interfaces with a cluster formed by 74 iron atoms distributed in three consecutive layers of 25, 24 and 25 metallic atoms and 74 palladium atoms distributed in a similar way (see Fig. 1). We have found that for cluster bigger than 50 metal atoms the results are stable and not depend of the cluster size [24]. The spacing between layers is 1.43 and 1.94 Å for Fe and Pd respectively (as in the bulk metals).

As in our previous paper we have selected a limit model for the interface with the purpose to find the optimal Fe–Pd interfacial distance [25]. All the coordinates along the [001] and [1$\bar{1}$0] axis were varied at 0.01 Å steps. The minimum interfacial distance is 1.73 Å. The

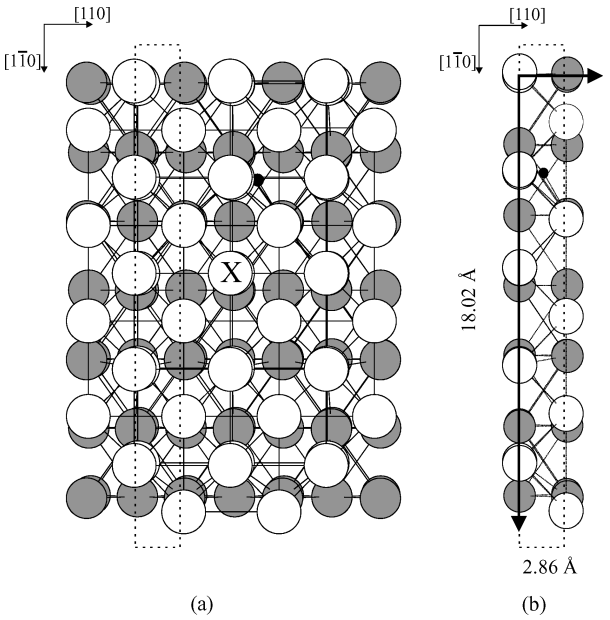

Figure 1 Schematics view of the $Fe_{74}Pd_{74}$ cluster (a) and Fe—Pd slab unit cell (b). The coordinate origin is marked with an X. The axis are referred to that of the Pd fcc structure. ● Fe ○ Pd ● H. The dashed line show the unit cell contain. The translations vector are also shown (b).

coordinate reference plane is located on the Pd layer nearest to the Fe layer (see Fig. 1). We have found no significative changes in the electronic structure and H localization when optimizing the distance within each layer.

We proceed to construct an H absorption model in the same manner as Jasen *et al*. [25]. When the H absorption on Fe(110)–Pd(100) interface is analyzed, the energy is mapped at planes parallels to the (110) surface. The H coordinates were varied at 0.01 Å step, while only first neighbor metallic atom relaxation allowed. For the sake of simplicity, when mapping the energy we have chosen only two highly dense planes and one additional plane in the middle of them.

The cluster configuration was also used to calculate adhesion energy.

2.2. Fe(110)–Pd(100) slab

The thickness of the Fe(110)–Pd(100) slab was chosen of six layer-width to make comparable with the $Fe_{74}Pd_{74}$ cluster. The unit cell of $^{2}_{\infty}[Fe_{21}$–$Pd_{15}]$ is shown schematically in Fig. 1b. Crystal grows along [110] and [1–10] axis reproduce the cluster surface. The interlayer spacing here is the same as in the cluster described before. Metallic layers orientation were chosen to match each other.

The H was located at the same metallic environment, found previously for the cluster case.

2.3. Fe–Pd alloys

The equiatomic Fe–Pd alloys can develop a poly-twinned microstructure after it undergoes the atomic ordering transformation. During the atomic ordering, the high temperature face-centered cubic (fcc) phase transform into a low temperature face-centered tetragonal (fct) phase which has a c/a ratio equal to ∼0.966 [26].

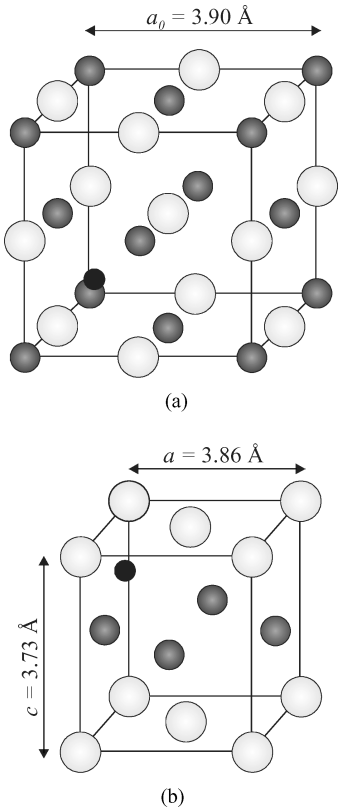

Figure 2 Fe─Pd alloys structures for fcc phase (a) and fct phase (b). The small black circles indicate the hydrogen atom locations. Light grey circles: Pd. Dark grey circles: Fe.

The high temperature phase has a fcc crystal structure which has a well known NaCl-type structure with a lattice parameter $a_0 = 3.90$ Å (see Fig. 2a).

The FePd ordered phase is isomorphic with the CuAu(I)-type structure with lattice parameters $a = 3.86$ Å and $c = 3.73$ Å (see Fig. 2b). The CuAu(I) structure has a primitive tetragonal Bravais lattice (P); hence it is also referred to in the literature as fct structure. In metallurgical nomenclature this structure is know as the $L1_0$ phase. The crystal space group is *P4/mmm*.

The H was located at the octahedral interstitial site according to Oriani [27] for the fcc structure. However, in the fct structure H was located at the tetrahedral interstitial site following the criteria described by Fukai [28].

3. Results and discussions

The H-cluster system result to be stable with energy minimum of −5.55 eV centered at (−2.71 Å, −0.97 Å). The H location is close to the interface near the first layer of Pd atoms (see Fig. 1). The H–Fe obtained distance is 1.34 Å and the H–Pd distance is 1.20 Å (see Fig. 3).

The adhesion energy curve is shows in Fig. 4. The shape of the energy curve is quite similar to that previously reported for Fe–Fe adhesion [16]. The minimum in the absorption energy is found at the interface, at the equilibrium distance (1.73 Å) between Fe and Pd layers.

Let us discuss the electronic structure of the Fe and Pd 3D solids and the Fe–Pd interface in absence of H. In the DOS of the bulk solids the metal d states form a band between −12 and −7 eV for Fe and between −13 and −10 eV for Pd. A similar bandwidth for Fe was reported by Griessen [29].

A substantial number of s and p states penetrate the d band. If we look at the detailed composition of, say a bulk like Fe atom in the slab we obtain the orbital population $d^{5.90}\ s^{0.55}\ p^{0.29}$, which is close to

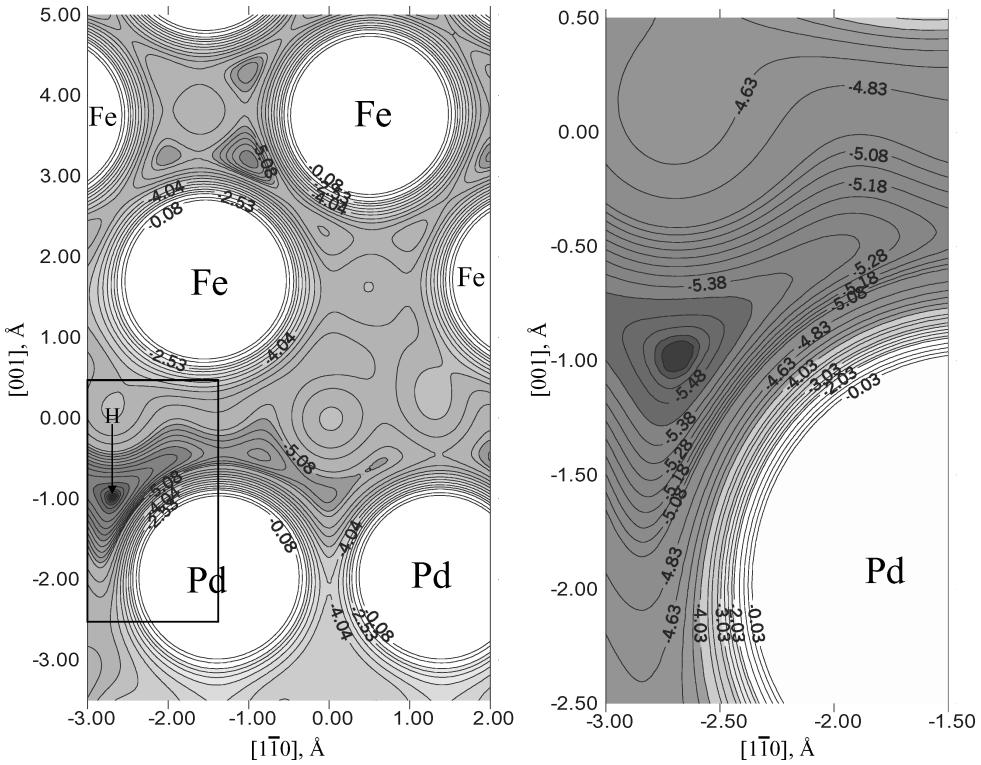

Figure 3 Contour energy curve corresponding to the cluster model for the Fe─Pd interface. Some energy values were deleted to allow better viewing. A zoom on the H region is added.

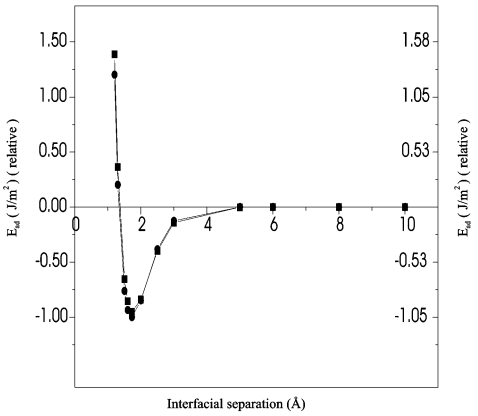

Figure 4 Curve of adhesion energy versus interfacial distance for the $Fe_{74}Pd_{74}$ cluster. ● Free cluster; ■ H–$Fe_{74}Pd_{74}$.

$d^{5.58}$ $s^{0.71}$ $p^{0.30}$ obtained for bulk Fe. In the case of Pd the value for the orbital population is $d^{9.57}$ $s^{0.74}$ $p^{0.82}$ while for the 3D fcc solid is $d^{9.27}$ $s^{0.46}$ $p^{0.27}$. The resulting Fermi energy (E_F) is −8.18 eV for the slab lies at an intermediate value closer to that of the Fe component.

The total DOS is almost the sum of the individual Fe and Pd components (Fig. 5). The Fe states are mixed with Pd states at the (−12, −9) eV range. The Pd states at the interface look only slightly changed with respect to the Pd bulk. It is known that a high DOS at the Fermi level causes the relatively high chemical activity of the TM and their alloys. Thus, the clean metallic surfaces cannot be inert.

Fig. 6 shows the COOP curves for the metal–metal bonds in the slab. At the interface the Fe–Pd COOP is 0.714 (see Table I). The Fe–Pd interaction seems to be strongly bonding.

3.1. The effect of H on the electronic structure

The total DOS is dominated by the contribution of Fe and Pd atoms. Fig. 7a looks similar to that of the slab without H (Fig. 5), except to a small peak at −16.65 eV. This peak appears right below the Fe *d* and Pd *d* bands and corresponds to the interaction of an H 1*s* orbital with Fe 4s and Pd 5s and 5p orbitals. The orbital composition is approximate Fe 3d 4%, 4s 15% and 4p 5%, Pd 4d 6%, 5s 18% and 5p 3%, and H 1s 58%. The interstitial H influences the electronic states of the closer Fe and Pd atoms. Second neighbors are almost unaltered.

Both metal–metal overlap population (OP), Fe–Fe and Pd–Pd, diminished with respect to the slab without H, as shown in Table I. The Fe–Fe bond OP decrease 64% and the Pd–Pd OP 49%. However, the interfacial Fe–Pd bond was only reduced by 27%. From the orbital population analysis it should be noted that the hydrogen affects mainly the Fe 4p orbitals. In the case of Pd the d orbitals seem to be more involved in the bond. Regarding the bonding the COOP curves in Fig. 8 show

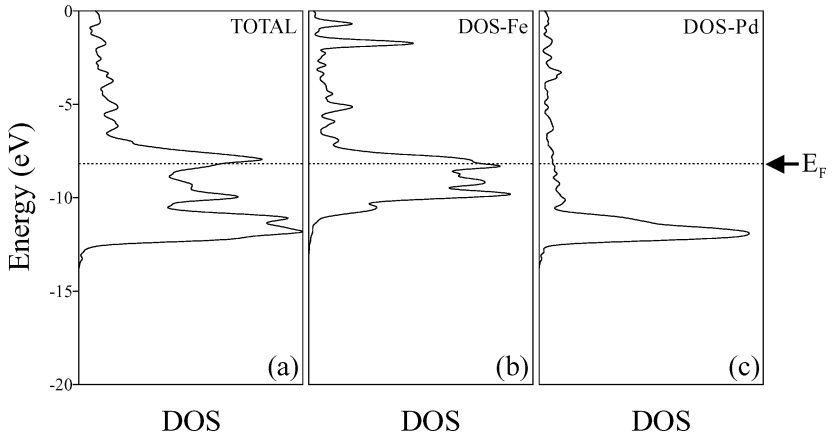

Figure 5 Total DOS curves for Fe—Pd slab (a). Projected DOS on a Fe atom first neighbor to the interface (b) and on a Pd atom (c).

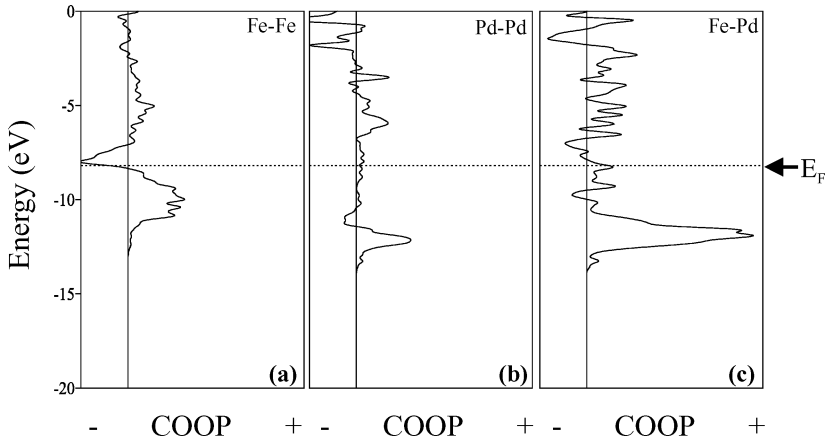

Figure 6 Fe—Pd COOP curves for the slab. Fe—Fe (a), Pd—Pd (b) and Fe—Pd (c) first neighbors.

TABLE I Electron density, overlap population, charge and distances for the Fe—Pd slab

Structure		Electron density			Charge	OP[1]	% Δ(OP)[2]	Distance (Å)	E_F (eV)
		s	*p*	*d*					
FePd slab									
Fe layer		0.55	0.29	5.90	1.253	0.367		2.478	−8.18
Fe—Pd	Fe	0.60	0.34	5.61	1.451	0.714		1.800	
	Pd	0.76	0.83	9.54	−1.123				
Pd layer		0.74	0.82	9.57	−1.138	0.147		2.751	
FePd—H slab									
H—Fe	H	1.23	0.00	0.00	−0.227	0.259		1.337	−7.94
	Fe	0.57	0.08	5.94	1.411				
H—Pd	H	1.23	0.00	0.00	−0.227	0.536		1.204	
	Pd	0.70	0.86	9.18	−0.740				
Fe layer		0.67	0.27	5.90	1.164	0.133	63.8	2.478	
Fe—Pd	Fe	0.67	0.14	6.00	1.185	0.523	26.7	1.908	
	Pd	0.83	0.84	9.21	−0.889				
Pd layer		0.86	0.88	9.27	−1.023	0.075	49.0	2.751	
Fe 3D		0.71	0.30	5.58	–	0.261	–	2.478	−7.79
Pd 3D		0.46	0.27	9.27	–	0.102	–	2.751	−10.66

[1]OP: Overlap population.
[2]%Δ(OP): Percentage change in the OP of a specified bond when H is absorbed.

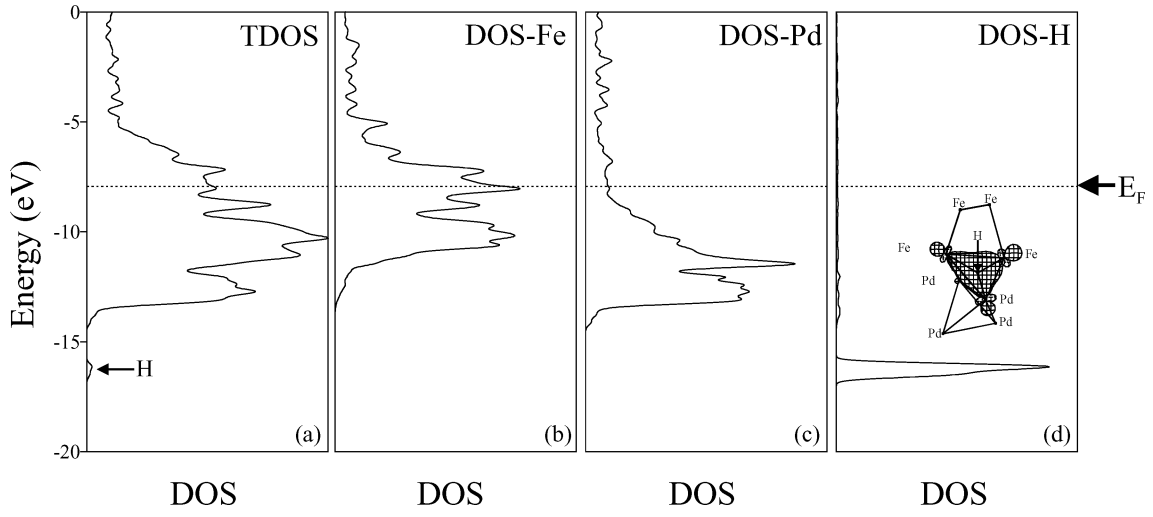

Figure 7 DOS curves for Fe—Pd slab. Total (a), PDOS Fe (b) and PDOS Pd (c) first neighbors to H, and PDOS for H (d). The insert in (d) shows the shape of H orbital 1a at −16.65 eV.

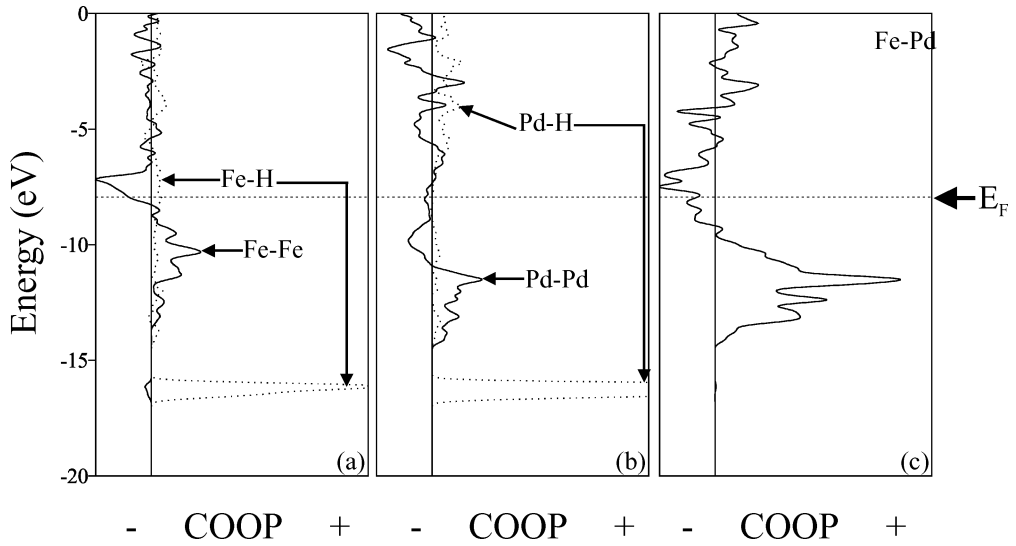

Figure 8 COOP curves for Fe—Pd slab after H adsorption. Fe—Fe and Fe—H (a), Pd—Pd and Pd—H (b), and Fe—Pd (c) first neighbors.

TABLE II Electron density, overlap population, charge and distances for FePd fcc structure

Structure		Electron density *s*	*p*	*d*	Charge	OP[1]	% Δ(OP)[2]	Distance (Å)	E_F (eV)
FePd fcc									
Fe layer		0.59	0.00	6.56	0.863	0.200		2.760	−7.27
Fe—Pd	Fe	0.69	0.00	6.54	0.867	0.368		1.952	
	Pd	0.82	0.89	9.15	−0.863				
Pd layer		0.82	0.89	9.15	−0.863	0.034		2.760	
FePd—H fcc									
H—Fe	H	1.16	0.00	0.00	−0.165	0.104		1.690	−7.40
	Fe	0.51	0.11	6.31	1.070				
H—Pd	H	1.16	0.00	0.00	−0.165	0.195		1.690	
	Pd	0.77	0.82	9.40	−0.995				
Fe layer		0.51	0.10	6.31	1.076	0.000	0.00	2.760	
Fe—Pd	Fe	0.51	0.10	6.31	1.076	0.286	22.3	1.952	
	Pd	0.77	0.82	9.40	−0.995				
Pd layer		0.76	0.82	9.40	−0.984	0.000	0.00	2.760	

[1]OP: Overlap population.
[2] %Δ (OP): Percentage change in the OP of a specified bond when H is absorbed.

bonding interaction at −15.95 eV for H–Fe and H–Pd. The Pd–Pd COOP changes with H. The bottom of the band is bonding (−10.90, −14.45) eV and the top antibonding, reflecting the decrease in the OP values. The interfacial bond shows antibonding contribution near the E_F, not present before (compare Figs 6c and 8c).

The adhesion energy shows no significative differences with that obtained from the minimum in Fig. 4. It has only a slight change in the minimum value for the energy. It is in fact well known that impurities can affect adhesion (for a review, see Smith *et al.* [30]). As an example of the role of impurities in adhesion see Smialek *et al.* [31] or Raynolds *et al.* [32]. In all cases, the impurities significantly lower electron densities accumulated between both metal at the interface. This suggests that the impurities are weakening those bonds. At the same time, the impurities are forming new bonds across the interface. There are competing effects. The adhesion energy is slightly reduced with respect to the clean interface (see Fig. 4).

3.2. Fe–Pd alloys structures

In both alloys structures the total charge is zero. It means that the charge has an equitative distribution between the components according to the infinite 3D solids.

An important difference between the slab and the fcc structures has been found. In the latter, the *d* orbital contributes much more for the Fe orbital population while the *p* orbital does not contribute at all (see Table II). This behavior is not observed for the Pd layer. The fct structure shows no significative differences with the slab value for Pd layer orbital population (Table III).

The Pd OP has a notorious decrease for the fcc structure with respect to the slab case for similar Pd–Pd distances (∼77%) while for the fct structure this decrease is only about of 12%. This can be understood by simple geometrical arguments. Remember that in the fcc structures (NaCl-type), the Fe and the Pd atoms have alternated positions at the unit cell. The Fe–Fe bond is less affected (∼45% for fcc and ∼41% for fct case) although the distances are not similar. The intermetallic

TABLE III Electron density, overlap population, charge and distances for FePd fct structure

Structure		Electron density *s*	*p*	*d*	Charge	OP[1]	% Δ(OP)[2]	Distance (Å)	E_F (eV)
FePd $L1_0$									
Fe layer		0.63	0.22	5.98	1.172	0.217		2.802	−8.46
Fe—Pd	Fe	0.63	0.22	5.98	1.172	0.185		2.721	
	Pd	0.85	0.77	9.54	−1.172				
Pd layer		0.85	0.77	9.54	−1.172	0.129		2.802	
FePd—H $L1_0$									
H—Fe	H	1.27	0.00	0.00	−0.271	0.037		1.931	−8.39
	Fe	0.54	0.10	6.20	1.159				
H—Pd	H	1.27	0.00	0.00	−0.271	0.214		1.866	
	Pd	0.71	0.78	9.53	−1.022				
Fe layer		0.47	0.21	5.96	1.348	0.157	27.6	2.802	
Fe—Pd	Fe	0.47	0.21	5.96	1.348	0.186	0.54	2.721	
	Pd	0.85	0.77	9.59	−1.214				
Pd layer		0.85	0.77	9.59	−1.214	0.126	2.32	2.802	

[1]OP: Overlap population.
[2]%Δ(OP): Percentage change in the OP of a specified bond when H is absorbed.

TABLE IV Parameters for ASED-MO and EHTB calculations

Atom	Orbital	Ionization potential (eV)	Slater exponent (au^{-1})	Linear coefficient	Electronegativity (Pauling)
H	1s	13.60	1.00		2.1
Fe	3d	9.00	5.35	0.5366	1.8
			1.80	0.6678	
	4s	7.87	1.70		
	4p	4.10	1.40		
Pd	4d	11.46	5.983	0.5264	2.2
			2.613	0.6373	
	5s	9.02	2.19		
	5p	5.557	2.152		

bondings OP decrease with respect to the slab interface (∼48% in fcc and ∼74% in fct case).

Near the Fermi level minimal bonding is shown which is comparable to the slab case.

When H is introduced as an interstitial, the H–Pd and Fe–Pd are the stronger bonds. As mentioned by Zhang *et al*. [14] and Karger *et al*. [33], there is a strong repulsive force between the Fe and any nearest neighbor H atoms in Pd–Fe alloys. The Fe–Fe and Pd–Pd interaction decrease because of the structure itself force the atoms to be more distant that in the slab case.

The Fe–Pd intermetallic bond in the slab structure is about 51% higher than the value in the fcc alloy structure. The H reduce it by 22% (see Table II). In the case of fct structure there are a small increase in the Fe–Pd OP after H absorption.

4. Conclusions

In this paper we have described the metal–metal adhesion and H absorption at the Fe–Pd interface. There is a strong bonding interaction between Fe and Pd layers, which is slightly affected by H due to its local effect.

The impurity tend to push the two surfaces apart slightly. This tends to weaken the metallic bonds that were there in the clean interface. It is evident that the impurity reduce the adhesion. This is a strong effect leading to a small decrease in adhesive energy (due to the small amount of H).

The H forms bonds with Fe and Pd atoms weakening the Fe–Fe and Pd–Pd cohesion. When alloys structures are considered it produces a notorious detrimental effect in the Pd–Pd bonds (fcc phase) while for the fct phase, the decrease in OP is only about 12% for the same bond.

Acknowledgements

The authors thank G. Brizuela and O. Nagel for their useful suggestions and to professor C. Mealli for providing us with the CACAO program. Ours work was supported by UNS-Física, Fundación Antorchas and ANPCyT (PICT 12-09857B). A Juan and N Castellani are members of CONICET. EA Gonzalez and PV Jasen are fellows of CONICET and CIC-Pcia de Bs As respectively. We thank valuable comments of the referees.

Appendix

The energies and optimised positions for the Fe–Pd–H system were calculated with a cluster approximation using the semi-empirical molecular orbital ASED-MO method, which predicts molecular structures from atomic data (atomic wave functions and ionisation potentials). This method is quite approximate but it is used because it provides a qualitative picture of Fe–Pd, Fe–H and H–Pd interactions.

Parameters necessary for calculations are listed in Table IV. Experimental values for ionisation potentials where taken from spectroscopic data [34]. The values for Slater exponent were those optimised by Nath and Anderson for describing Fe–Fe [35] and Vela and Gázquez or Basch and Gray [36, 37] for Pd–Pd bulk interaction.

The ASED-MO method is a modification of the Extended Hückel method that includes a repulsive term for the electrostatic interaction between nucleus [38]. The energy was computed as the difference ΔE between the Fe–Pd–H composite system when the H atom is absorbed at a specified geometry and when it is far away from the Fe–Pd interface. It can be expressed as

$$\Delta E_{\text{Total}} = E(\text{H} - \text{Fe}_{74}\text{Pd}_{74}) - E(\text{Fe}_{74}\text{Pd}_{74}) - E(\text{H}) + E_{\text{repulsion}}$$

where E is the electronic energy, $E_{\text{repulsion}}$ is the repulsive energy for nucleus j in the presence of a fixed atom i:

$$E_{\text{repulsion}} = \frac{1}{2}\sum_i \sum_{j \neq i} E_{ij}$$

(E_{ij} is a pair wise electrostatic term). The summation extends over all Fe–Fe, Pd–Pd, H–Fe and H–Pd pairs.

To understand the Fe–Pd–H interaction we used the concept of DOS (density of states) and COOP (crystal orbital overlap population) curves implemented with the program YAeHMOP [39]. The DOS curve is a plot of the number of orbital per unit volume per unit energy. The COOP curve is a plot of the overlap population weighted DOS vs. energy. The integration of the COOP curve up to the Fermi level (E_{F}) gives the total overlap population of the bond specified and it is a measure of the bond strength. A positive value of COOP means bonding interactions while a negative value represent antibonding interactions of a specified bond or orbital.

Due to the approximate nature of the ASED-MO method the reported values for the energy should be interpreted in their *relative* terms.

The molecular orbital showed in Fig. 7 and the percentage orbital population were done using the CACAO computer package [40].

References

1. D. WANG, T. B. FLANAGAN and R. BALASUBRAMANIAM, *J. Alloys Comp.* **364** (2004) 105.
2. D. S. DOS SANTOS, V. M. AZAMBUJA, L. PONTONNIER, S. MIRAGLIA and D. FRUCHART, *ibid.* **356/357** (2003) 236.
3. S. SEMBOSHI, N. MASAHASHI and S. HANADA, *ibid.* **352** (2003) 210.
4. S. M. MYERS, M. I. BASKES, H. K. BIRNBAUM, J. W. CORBETT, G. G. DE LEO, S. K. ESTREICHER, E. E. HALLER, P. JENA, N. M. JOHNSON, R. KIRCHHEIM, S. J. PEARTON and M. J. STAVOLA, *Rev. Mod. Phys.* **64** (1992) 559.
5. Y. HAYASHI, W. M. SHU, T. SHIRAISHI and M. MASUDA, *J. Alloys Comp.* **231** (1995) 291.
6. B. F. P. ROOS, A. R. FRANK, S. O. DERMOKRITOV and B. HILLERBRANDS, *J. Magne. Magn. Mat.* **198/199** (1999) 725.
7. J. GONIASKOWSKI and C. NOGIERA, *Phys. Rev. B* **60** (1999) 120.
8. E. LUNDGREN, M. QVARFORD, R. NYHOLM, J. N. ANDERSEN and D. HESKETT, *ibid.* **50** (1994) 4711.
9. B. HAMMER and M. SCHEFFER, *Phys. Rev. Lett.* **74** (1995) 3487.
10. G. BIHLMAYER, R. EIBLER and R. PODLOUCKY, *Surf. Sci.* **402/404** (1998) 794.
11. *Idem.*, *ibid.* **446** (2000) 188.
12. A. Y. LOZOVOI, A. ALAVI and M. FINNIS, *Phys. Rev. Lett.* **85** (2000) 610.
13. S. OSTAMIN, V. M. UZDIN, C. DEMANGEAT, J. M. WILLS, M. ALOUANI and H. DREYSSETT, *Phys. Rev. B* **61** (2000) 4870.
14. W. ZHANG, S. LUO and T. B. FLANAGAN, *J. Alloys Comp.* **293/295** (1999) 1.
15. T. HONG, J. R. SMITH and D. J. SROLOVITZ, *Phys. Rev. Lett.* **70** (1993) 615.
16. A. HUNG, I. YAROVSKY, J. MUSCAT, S. RUSSO, I. SNOOK and R. O. WATTS, *Surf. Sci.* **501** (2002) 261.
17. S. M. MAYERS, P. M. RICHARDS and W. R. WAMPLER, *J. Nucl. Mater.* **165** (1989) 9.
18. W. A. SWANSIGER and R. BASTAZ, *ibid.* **85/86** (1979) 335.
19. F. WAELBROECK, K. J. DIETZ, P. WIENHOLD, J. WINTER, I. ALI-KHAN, H. MERKENS and E. ROTA, *ibid.* **93/94** (1980) 839.
20. Y. HAYASHI, A. TAHARA and M. ISHIBASHI, in "Hydrogen Effects on Material Behavior in N.R. Mood" edited by A. W. Thompson (The Mineral, Metal and Material Society, Warrendale, PA, 1990) p. 11.
21. M. B. LOPEZ, G. L. ESTIÚ, E. A. CASTRO and A. J. ARVIA, *Surf. Sci.* **277** (1992) 184.
22. N. J. CASTELLANI, P. LÉGARÉ, C. DEMANGEAT, P. MIKUŠÍK and Š. PICK, *ibid.* **307/309** (1994) 927.
23. P. LÉGARÉ, N. J. CASTELLANI and G. F. CABEZA, *ibid.* **496** (2002) L51.
24. C. PISTONESI, A. GARCIA, G. BRIZUELA and A. JUAN, *J. Phys. D: Appl. Phys.* **31** (1998) 588.
25. P. V. JASEN, E. A. GONZALEZ, O. A. NAGEL and A. JUAN, *Surf. Rev. Lett.* **10**(6) (2003) 879.
26. *Constitution of Binary Alloys*, in "Metallurgy and Metallurgical Eng. Series," edited by M. Hansen (Mc Graw-Hill CO, 1958) p. 696 .
27. R. A. Oriani, "The Physical and Metallurgical Aspect of Hydrogen in Metals," in *ICCF4* (1993).
28. Y. FUKAI, "The Metal-Hydrogen System: Basic Bulk Properties" (Springer-Verlag, Berlin, 1993).
29. R. GRIESSEN, *Phys. Rev. B* **38** (1988) 3690.
30. J. R. SMITH and T. V. CIANCOLO, *Surf. Sci. Lett.* **210** (1989) L229.
31. J. L. SMIALEK, D. T. JAYNE, J. C. SCHAEFFER and W. H. MURPHY, *Thin Solids Films* **253** (1994) 285.
32. J. E. RAYNOLDS, E. R. RODDICK, J. R. SMITH and D. J. SROLOVITZ, *Acta Materialia* **47** (1999) 3281.
33. M. KARGER, F. PRÖBST, B. SCHÜTTLER and F. WAGNER, in "Metal-Hydrogen Systems," edited by T. Veziroglu (Pergamon Press, Oxford, 1982) p. 182.
34. G. HERTZBERG, "Spectra of Diatomic Molecules," 2nd edn. in Van Nostrand (Princeton, NJ, 1950).
35. K. NATH and A. B. ANDERSON, *Phys. Rev. B* **39** (1989) 1013.
36. A. VELA and G. L. GÁZQUEZ, *J. Chem. Phys.* **92** (1988) 5668.
37. M. BASCH and H. B. GRAY, *Theor. Chim. Acta* **4** (1966) 367.
38. A. B. ANDERSON, *J. Chem. Phys.* **62** (1975) 1187 .
39. G. A. LANDRUM and W. V. GLASSEY, *YAeHMOP Extended Hückel Molecular Orbital Package* is freely available on the WWW at http://sourceforge.net/projects/yaehmop/.
40. C. MEALLI and D. M. PROSPERIO, *J. Chem. Educ.* **27** (1988) 1593.